Universiteit Leiden
The Netherlands

Magnetic resonance imaging contrast-enhancement with superparamagnetic iron oxide nanoparticles amplifies macrophage foam cell apoptosis in human and murine atherosclerosis

Segers, F.M.E.; Ruder, A.V.; Westra, M.M.; Lammers, T.; Dadfar, S.M.; Roemhild, K.; ... ; Biessen, E.A.L.

Citation
Segers, F. M. E., Ruder, A. V., Westra, M. M., Lammers, T., Dadfar, S. M., Roemhild, K., … Biessen, E. A. L. (2022). Magnetic resonance imaging contrast-enhancement with superparamagnetic iron oxide nanoparticles amplifies macrophage foam cell apoptosis in human and murine atherosclerosis. *Cardiovascular Research*. doi:10.1093/cvr/cvac032

Version:	Corrected Publisher's Version
License:	Creative Commons CC BY-NC 4.0 license
Downloaded from:	https://hdl.handle.net/1887/3486254

Note: To cite this publication please use the final published version (if applicable).

ESC European Society of Cardiology

Cardiovascular Research (2022) **00**, 1–14
https://doi.org/10.1093/cvr/cvac032

Magnetic resonance imaging contrast-enhancement with superparamagnetic iron oxide nanoparticles amplifies macrophage foam cell apoptosis in human and murine atherosclerosis

Filip M.E. Segers [1,2], Adele V. Ruder[3], Marijke M. Westra[1], Twan Lammers[4], Seyed Mohammadali Dadfar[4], Karolin Roemhild[4,5], Tin Sing Lam[1], Marianne Eline Kooi [6], Kitty B.J.M. Cleutjens [3], Fons K. Verheyen[7], Geert W.H. Schurink[8], Guido R. Haenen [9], Theo J.C. van Berkel [1], Ilze Bot [1], Bente Halvorsen [2], Judith C. Sluimer [3,10]*†, and Erik A.L. Biessen [1,3,11]*†

[1]Division of BioTherapeutics, Leiden Academic Centre for Drug Research, Leiden, The Netherlands; [2]Faculty of Medicine, Research Institute of Internal Medicine, University Hospital Oslo, Oslo, Norway; [3]Department of Pathology, CARIM School for Cardiovascular Sciences, Maastricht University Medical Center, Maastricht, The Netherlands; [4]Department of Nanomedicine and Theranostics, RWTH Aachen University, Aachen, Germany; [5]Institute of Pathology, RWTH Aachen University, Aachen, Germany; [6]Department of Radiology and Nuclear Medicine, CARIM School for Cardiovascular Sciences, Maastricht University Medical Center, Maastricht, The Netherlands; [7]Molecular Cell Biology and Electron Microscopy (CRISP), Maastricht University Medical Center, Maastricht, The Netherlands; [8]Department of Surgery, CARIM School for Cardiovascular Sciences, Maastricht University Medical Center, Maastricht, The Netherlands; [9]Department of Toxicology, Maastricht University Medical Center, Maastricht, The Netherlands; [10]Cardiovascular Sciences, Edinburgh University, Edinburgh, UK; and [11]Institute for Molecular Cardiovascular Research, RWTH Aachen University, Aachen, Germany

Received 9 February 2020; accepted 23 February 2022; online publish-ahead-of-print 23 March 2022

Aims (Ultra) Small superparamagnetic iron oxide nanoparticles, (U)SPIO, are widely used as magnetic resonance imaging contrast media and assumed to be safe for clinical applications in cardiovascular disease. As safety tests largely relied on normolipidaemic models, not fully representative of the clinical setting, we investigated the impact of (U)SPIOs on disease-relevant endpoints in hyperlipidaemic models of atherosclerosis.

Methods and results RAW264.7 foam cells, exposed *in vitro* to ferumoxide (dextran-coated SPIO), ferumoxtran (dextran-coated USPIO), or ferumoxytol [carboxymethyl (CM) dextran-coated USPIO] (all 1 mg Fe/mL) showed increased apoptosis and reactive oxygen species accumulation for ferumoxide and ferumoxtran, whereas ferumoxytol was tolerated well. Pro-apoptotic ($TUNEL^+$) and pro-oxidant activity of ferumoxide (0.3 mg Fe/kg) and ferumoxtran (1 mg Fe/kg) were confirmed in plaque, spleen, and liver of hyperlipidaemic $ApoE^{-/-}$ ($n = 9$/group) and $LDLR^{-/-}$ ($n = 9$–16/group) mice that had received single IV injections compared with saline-treated controls. Again, ferumoxytol treatment (1 mg Fe/kg) failed to induce apoptosis or oxidative stress in these tissues. Concomitant antioxidant treatment (EUK-8/EUK-134) largely prevented these effects *in vitro* (−68%, $P < 0.05$) and in plaques from $LDLR^{-/-}$ mice (−60%, $P < 0.001$, $n = 8$/group). Repeated ferumoxtran injections of $LDLR^{-/-}$ mice with pre-existing atherosclerosis enhanced plaque inflammation and apoptosis but did not alter plaque size. Strikingly, carotid artery plaques of endarterectomy patients who received ferumoxtran (2.6 mg Fe/kg) before surgery ($n = 9$) also showed five-fold increased apoptosis (18.2 vs. 3.7%, respectively; $P = 0.004$) compared with controls who did not receive ferumoxtran. Mechanistically, neither coating nor particle size seemed accountable for the observed cytotoxicity of ferumoxide and ferumoxtran.

Conclusions Ferumoxide and ferumoxtran, but not ferumoxytol, induced apoptosis of lipid-laden macrophages in human and murine atherosclerosis, potentially impacting disease progression in patients with advanced atherosclerosis.

Keywords Apoptosis • Atherosclerosis • Leucocyte • Oxidative stress • Iron oxide nanoparticles

* Corresponding author. Tel: +31 43 3877675; Fax: +31 43 3874613, E-mail: judith.sluimer@maastrichtuniversity.nl (J.C.S.); E-mail: erik.biessen@mumc.nl (E.A.L.B.)
† These authors contributed equally to the study.

Published on behalf of the European Society of Cardiology. © The Author(s) 2022.
This is an Open Access article distributed under the terms of the Creative Commons Attribution-NonCommercial License (https://creativecommons.org/licenses/by-nc/4.0/), which permits non-commercial re-use, distribution, and reproduction in any medium, provided the original work is properly cited. For commercial re-use, please contact journals.permissions@oup.com

Downloaded from https://academic.oup.com/cardiovascres/advance-article/doi/10.1093/cvr/cvac032/6553202 by Jacob Heeren user on 09 November 2022

1. Introduction

Functional imaging is widely employed to detect rupture-prone atherosclerotic plaques in coronary artery disease and carotid artery disease patients at risk of clinical symptoms.[1] Rupture-prone plaques are typified by extensive lipid deposition, inflammation, matrix degradation, and cell death. These factors eventually lead to fibrous cap rupture and subsequent formation of an atherothrombus.[2,3]

Several passive and active molecular imaging modalities have been considered to identify high-risk plaques, including ^{18}F-fluoro-deoxyglucose-guided positron emission tomography–computed tomography (PET–CT), marking plaque inflammation and contrast-enhanced magnetic resonance imaging (MRI), respectively. MRI offers the advantage of superior spatial resolution, especially when using small [50–150 nm; small superparamagnetic iron oxide nanoparticles (SPIO)] and ultrasmall superparamagnetic iron oxide nanoparticles (15–30 nm; USPIO) to enhance signal contrast.[4–10] Upon systemic administration, both formulations are rapidly cleared by the reticulo-endothelial system of lung and liver and by renal excretion, while accumulation in heart and brain is less pronounced, maximizing signal to noise.[11] USPIO extravasation and uptake by macrophages are considerably increased in inflammation,[12–14] and vascular macrophages in the atherosclerotic plaque, in the abdominal aneurysm, and in the infarcted or inflamed heart show avid accumulation of these particles,[4,5,15–20] rendering them useful for cardiovascular disease (CVD) imaging.

Extensive toxicology studies led to the assumption that (U)SPIO are safe for clinical application.[21–23] However, this notion is merely based on studies in normolipidaemic animal and cell culture models. In the hyperlipidaemic setting of atherosclerosis, vascular macrophages will acquire a foam cell phenotype, with intracellular free cholesterol deposits, and increased production of reactive oxygen species (ROS) and susceptibility to apoptosis.[24,25] Moreover, upon uptake USPIO will accumulate in endo-lysosomes, where their coating will be degraded and the entrapped iron oxide cargo released.[26,27] Besides prolonging the imaging signal,[26,27] this will also foster an oxidative stress response, which may well be detrimental to macrophage survival. Moreover, monocyte-derived macrophages were reported to enhance inflammatory cytokine secretion upon exposure to iron oxide particles.[28] This suggests that (U)SPIO toxicity data obtained in normolipidaemic, inflammatory macrophages *in vitro* may not be representative of the clinical situation. This prompted us to study (U)SPIO in macrophage foam cells, and in murine and human atherosclerosis to elucidate potentially unfavourable effects under clinically relevant conditions.

2. Methods

2.1 Cell culture

The RAW264.7 murine macrophage cell line was grown in DMEM, containing 10% foetal bovine serum (heat-inactivated for 30 min at 56°C), 2 mmol/L L-glutamine, 100 U/mL penicillin, and 100 µg/mL streptomycin (all from PAA, Cölbe, Germany), at 37°C in a humidified atmosphere (5% CO_2).

Human very low-density lipoprotein (hVLDL) was isolated from the human serum of healthy volunteers by discontinuous density gradient centrifugation (using KBr; 40 000 rpm for 22 h).[29] The VLDL fraction was collected and dialyzed against phosphate-buffered saline containing 1 mM ethylenediaminetetraacetic acid. RAW264.7 cells were incubated with hVLDL (50 µgmL) for 20 h and replaced by medium with or without ferumoxide (100 µg Fe/mL, Guerbet) or two types of ultrasmall iron oxide nanoparticles (100 µg Fe/mL): ferumoxtran (Guerbet, France), and ferumoxytol (RIENSO, Takeda, EU tradename for feraheme, AMAG Pharmaceuticals, MA, USA). Cells were pre-treated with EUK-8 antioxidant 2 h prior to ferumoxtran treatment (25 µM; Merck Chemicals Ltd., Nottingham, UK). Viability of RAW cells was assessed using MTT assay [3-(4,5-dimethylthiazol-2-yl)-2,5-diphenyl-tetrazolium-bromide; Sigma]. Apoptosis was quantified in $\geq$3 fields per well, 20× magnification after terminal deoxynucleotidyl transferase deoxyuridine triphosphate nick-end labelling (TUNEL) (Roche Diagnostics, Basel, Switzerland), or by flow cytometry of Annexin V-Oregon green (120 ng/mL).

2.2 Iron content

Ferumoxtran (100 µg Fe/mL) uptake by RAW264.7 macrophages and foam cells was determined after incubation for 1 h at 37°C. Quantitative determination of iron uptake by inductively coupled plasma atomic emission spectroscopy (Optima 3300 RL, Perkin Elmer, Courtaboeuf, France) was carried out after mineralization of the pellet with HNO_3 (3 h at 80°C).

2.3 Animals and tissue harvesting

All animal work was performed in compliance with the Dutch government and Directive 2010/63/EU guidelines and approved by national and local review boards (AVD1070020185705). Male LDL receptor knockout (LDLR$^{-/-}$) or Apolipoprotein E knockout (ApoE$^{-/-}$) mice (aged 12 weeks) were obtained from the local animal facility. Animals were housed in the laboratory animal facility of Leiden University under standard conditions. Food and water were provided *ad libitum* during the entire experiment. All animals were housed in individually ventilated cages (GM500, Techniplast) in groups of up to five animals per cage, with bedding (corncob, Technilab-BMI) and cage enrichment. Cages were changed weekly, reducing handling of the mice to one handling per week during non-intervention periods.

A pilot study was done with ApoE$^{-/-}$ mice (n = 3/group) that received a single dose of saline, ferumoxide (0.3 mg Fe/kg), or ferumoxtran (1 mg Fe/kg) after 9 weeks on a western-type diet (WTD, 0.25% cholesterol, 15% cocoa butter, SDS, Sussex, UK). Based on this, a sample size of eight single mice per group was calculated by power analysis. No inclusion or exclusion criteria were set. Cages were randomly located on the racks. LDLR$^{-/-}$ (n = 9/group) were fed a WTD for 3 weeks, after which they received weekly intravenous (IV) injections of saline or ferumoxtran and fed a WTD for five consecutive weeks. LDLR$^{-/-}$ (n = 8/group) fed a WTD for 14 weeks received either saline, ferumoxtran, antioxidant EUK-134 (10 mg/kg, Cayman Chemicals, Ann Arbor, MI, USA), or ferumoxtran with EUK-134, whereby EUK-134 was administered intraperitoneally 1 h prior to the IV injection of ferumoxtran. In a third experiment, male LDLR$^{-/-}$ (n = 9/group) fed a WTD for 9 weeks received a single saline, or ferumoxytol (1 mg Fe/kg) injection. In all experiments, 24 h after the final injection, mice were anaesthetized using a single dose of pentobarbital (100 mg/kg i.p.), subjected to blood sampling and *in situ* perfusion-fixation through the left cardiac ventricle. Aortic root, liver, and spleen were collected for cryosectioning using a Leica CM 3050S Cryostat (Leica Instruments, Nassloch, Germany).

2.4 Human tissue collection

Atherosclerotic carotid arteries (n = 18) were obtained at surgery from patients treated with ferumoxtran (2.6 mg Fe/kg, single dose, n = 9) and historic control patients (n = 9) matched for age, sex, and plaque type (*Table 1*) to analyse apoptosis in plaque sections.[4] Inclusion and

Downloaded from https://academic.oup.com/cardiovascres/advance-article/doi/10.1093/cvr/cvac032/6553202 by Jacob Heeren user on 09 November 2022

Table 1 Patient characteristics

Patient characteristics		Control ($n=9$)	Ferumoxtran ($n=9$)
Gender	% male; male/female	89%; 8/1	89%; 8/1
Age	Years ± SD	64.6 ± 2.9	63.9 ± 3.2
Plaque type	Thin/thick cap fibroatheroma	67% ($n=6$)	67% ($n=6$)
	Intraplaque/luminal thrombus	33% ($n=3$)	33% ($n=3$)
Clinical stage	% symptomatic	100%	100%
Stenosis	Percentage patients with >70%	100%	100%

No significant *P*-values.

exclusion criteria were described before.[4] Sample size was calculated based on interpatient MRI enhancement. Collection, storage, and use of tissue and patient data were performed in agreement with institutional ethical guidelines and the principles outlined in the Declaration of Helsinki, and approved by the Maastricht University Medical Center Medical Ethical Committee (MEC00-078b).[4] Subjects gave informed consent prior to the inclusion and were enrolled consecutively between 2000 and 2002. Samples were processed and classified based on plaque morphology as described previously.[30]

2.5 Histology and morphometry

Aortic root cryosections (10 μm) were stained with Oil Red O (Sigma) and MoMa-2 (1: 50; Serotec, Oxford, UK) to detect lipid deposits and macrophage content, respectively. Secondary antibody goat anti-rat IgG-AP (1:100; Sigma, St-Louis, MO, USA) and enzyme-substrate nitro-blue tetrazolium chloride with 5-bromo-4-chloro-3′-indolyphosphate p-toluidine salt (DAKO, Glostrup, Denmark) were used for MoMa-2 visualization. The primary outcome of apoptotic cells in liver, spleen, and atherosclerotic plaque was detected using TUNEL (Roche Diagnostics, Basel, Switzerland) and visualized using Nova-Red (DAKO) for mouse and AEC (Sigma) for human sections. Human atherosclerotic plaques were stained with 8OH-dG (Japan Institute for the Control of Aging, clone N45.1), TUNEL, and cleaved caspase for apoptosis, CD68 to detect ROS, apoptosis, and macrophages, respectively. Quantitative morphometric analysis of Oil Red O, MoMa-2, and TUNEL was performed using Leica Qwin image analysis software and a Leica-DM-RE microscope (Leica Imaging Systems, Cambridge, UK). Cells were marked as apoptotic when double positive for TUNEL and DAPI. High-sensitive Perl's iron staining was performed to visualize iron nanoparticles. Following quenching of endogenous peroxidases by hydrogen peroxide (0.3% in methanol), slides were incubated for 90 min in 1:1 solution of 2% HCl + 2% potassium hexacyanoferrate Fe^{2+}. After washing, slides were incubated for 20 min in 3,3′-diaminobenzidine (DAB, DAKO). Slides were counterstained with nuclear fast red. Negative control sections incubated with DAB only were negative. Outcome and data analysis were done blindly.

2.6 Electron microscopy

Tissue fragments of carotid endarterectomy specimens of ~1 mm^3 were fixed overnight in 2.5% glutaraldehyde (Ted Pella, Redding, CA, USA), post-fixed in 1% osmium tetroxide solution, dehydrated, and embedded in epoxy resin. Semi-thin (1 μm) serial sections were stained with toluidine blue to localize microvessels. Ultra-thin sections (70–90 nm) were mounted on Formvar (1595 E, Merck)-coated 75 mesh copper grids, and counterstained with uranyl acetate and lead citrate before analysis on a Philips CM100 transmission electron microscope.

2.7 Trolox equivalent antioxidant capacity

The trolox equivalent antioxidant capacity (TEAC) gives the concentration of 2,2′-azino-bis (3-ethylbenzthiazoline-6-sulfonic acid) diammonium salt (ABTS) radicals that can be scavenged by serum. It is a measure of antioxidant capacity. The TEAC was determined in serum that was deproteinated with a final concentration of 5% trichloroacetic acid (TCA) as described.[31] The samples were incubated with an ABTS radical solution for 5 min and subsequently, the reduction in absorbance at 734 nm, reflecting the extent of radical scavenging, was quantified. This is related to that of the reference antioxidant trolox and is expressed as μM trolox equivalents. The TEAC value gives the concentration of trolox that has the same capacity.

2.8 Uric acid

Uric acid was determined in serum that was deproteinated with a final concentration of 5% TCA, using high-performance liquid chromatography. A Hypersil BDS C-18 end-capped column, 125 × 4 mm, particle size 5 μm (Agilent, Palo Alto, CA, USA), was used, with a mobile phase of 0.1% trifluoroacetic acid (v/v) in water. UV detection was performed at 292 nm.

2.9 IL-1β ELISA

IL-1β, secreted in the supernatant medium of RAW cells, was measured as suggested by the manufacturer (Invitrogen, Breda, The Netherlands).

2.10 Quantitative RT–PCR

Quantitative RT–PCR analysis was performed to determine mRNA expression of apoptosis and oxidative stress-related genes in RAW cells, foam cells, and ferumoxtran-treated foam cells. Total RNA extracts isolated using the guanidium isothiocyanate method[32] were transformed into cDNA using RevertAid M-MuLV reverse transcriptase (Fermentas, Burlington, Canada) according to the manufacturer's protocol. Quantitative gene expression analysis was performed with the SYBR-Green technology on a 7500 fast Real-Time PCR apparatus (Applied Biosystems, Foster City, CA, USA). All Ct values were normalized to the stable-expressed reference gene hypoxanthine phospho-ribosyltransferase. Supplementary material online, *Table S1* shows a detailed overview of the different primer pairs (Eurogentec, Maastricht, The Netherlands), which were designed using NCBI primer blast.

2.11 Serum cholesterol analysis

Total cholesterol concentration in serum was determined using an enzymatic colorimetric assay (Roche Diagnostics). Precipath I (Roche Diagnostics) was used as an internal standard. Absorbance was measured at 490 nm. Cholesterol distribution over the different lipoprotein fractions was determined by fractionation of 30 μL serum using a Superose 6 column (3.2 × 300 mm, Smart-system, Pharmacia, Uppsala, Sweden). Cholesterol content of the effluent was determined as described above.

2.12 Dextran uptake assay

RAW264.7 cells were seeded at 75 000 cells per well in a 96-well black clear-bottom imaging microplate (Corning #353219) in DMEM medium with 4.5 g/L D-glucose and pyruvate (Gibco #31966-021) supplemented with 10% heat-inactivated (30 min at 56°C) foetal bovine serum

Downloaded from https://academic.oup.com/cardiovascres/advance-article/doi/10.1093/cvr/cvac032/6553202 by Jacob Heeren user on 09 November 2022

(SERANA S-FBS-SA-015) and 1% penicillin–streptomycin, and left to attach for 2 h (37°C, 5% CO_2). The supernatant of cells was either replaced with 1, 2.4, or 4 μM tetramethylrhodamine isothiocyanate (TRITC)-labelled dextran (ThermoFisher Scientific #D7139). After 1 h (37°C, 5% CO_2), cells were washed with DMEM and nuclei were stained with Hoechst 33342 (Sigma #B2261) in DMEM for 10 min (37°C, 5% CO_2). Cells were imaged using the BD Pathway 855 (BD Biosciences) and analysed with CellProfiler software 4.0.4.[33]

2.13 Chemicals for the synthesis of iron particles

Ferric chloride anhydrous, ferrous chloride tetrahydrate, 1,10-phenanthroline, hydroxylamine hydrochloride, dextran, and CM dextran were purchased from Sigma–Aldrich (Munich, Germany). Trisodium citrate dihydrate, citric acid, hydrogen chloride, ammonium hydroxide (NH_4OH), and sodium hydroxide were obtained from Carl Roth (Karlsruhe, Germany).

2.14 Synthesis of citrate-coated iron particles

Citrate-coated iron particles were prepared via the standard co-precipitation technique. Briefly, 8 mmol of ferric chloride was dissolved in 10 mL of deionized water (from here on water) and mixed for 5 min under mechanical stirring and nitrogen atmosphere. Subsequently, 4 mmol of ferrous chloride tetrahydrate was added to the solution and mixed for a further 5 min at room temperature. The pH of the solution was adjusted to 11.0 by adding 80 mL of 1 M aqueous ammonia solution drop-wisely and vigorously stirred at room temperature for 30 min. The formed black-coloured iron oxide nanoparticles were decanted using a permanent magnet and washed at least three times with 500 mL of water. Afterwards, 20 mL of 0.1 M hydrochloric acid was added to the particles and sonicated for 10 min. Following, 2.5 g trisodium citrate dihydrate in 10 mL of water were added to the mixture and was stirred at 80°C for 2 h. The citrate-coated polydisperse particles were separated using a permanent magnet and then resuspended in 35 mL of water. Finally, the suspension was passed through a 0.2 μm filter to remove larger particles.

This highly polydisperse crude batch was subjected to five sequential rounds of centrifugation to obtain monodispersed iron particle subfractions. As depicted in Supplementary material online, *Figure S1*, the supernatant obtained after 20 min of centrifugation at 14 000 rpm is referred to as Citrate S (USPIO size). The precipitate was resuspended in water and centrifuged again at progressively lower speed. The monodisperse batch obtained after five centrifugation cycles is referred to as Citrate L (SPIO size).

2.15 Synthesis of dextran-coated iron particles

Dextran-coated iron particles were prepared via the standard co-precipitation technique, under a nitrogen atmosphere. Briefly, 1 mmol of ferric chloride was dissolved in 2 mL of water and mixed for 5 min under mechanical stirring and nitrogen atmosphere. Subsequently, 0.5 mmol of ferrous chloride tetrahydrate in 1 mL of water was added to the solution and mixed for 5 min at room temperature after which pH was adjusted to 11.0 (1 M aqueous ammonia). The suspension was stirred at 0°C for 1 or 30 min to obtain differently sized particles and an aqueous solution of dextran (1 or 10 kDa; 1 g) or CM dextran (10–20 kDa, 1 g), filtered over a 200 nm syringe filter, was added. The temperature was slowly increased to 80°C and was kept at that temperature for 60 min. Afterwards, the solution was cooled down to room temperature. The formed black-coloured iron oxide particles were sonicated for 20 min. Following, the solution was dialyzed for 24 h against 5 L of water (25 kDa cutoff, SnakeSkin™ dialysis membrane, ThermoFisher Scientific, MA, USA). Finally, the suspension was passed through a 0.2 μm filter to remove the aggregates. Also here, the highly polydisperse starting batch was fractionated by size via two sequential rounds of centrifugation as described above [14 000 rpm, 20 min (S batch) and 7000 rpm, 10 min (L batch)].

2.16 Characterization of synthesized iron particles

Particle size and size distribution, zeta potential, average hydrodynamic diameter (Dh), and polydispersity index of the particles were measured by dynamic light scattering using a Zetasizer Nano-ZS instrument (Malvern Instruments, Malvern, UK) at 25°C. The machine was equipped with a 633 nm He–Ne laser and a detector at an angle of 173°. The samples were diluted and sonicated in a water bath prior to size analysis. Iron concentration was measured using 1,10-phenanthroline assay as described previously.[34] Finally, the absorbance was detected at 510 nm using an Infinite M200 Pro TECAN reader (TECAN, Germany).

2.17 Apoptosis assay

RAW264.7 cells were seeded at 6000 cells per well in a 96-well black clear-bottom imaging microplate (Corning #353219) in DMEM medium with 4.5 g/L D-glucose and pyruvate (Gibco #31966-021) supplemented with 10% heat-inactivated (30 min at 56°C) foetal bovine serum (SERANA S-FBS-SA-015) and 1% penicillin–streptomycin, and left to attach for 24 h (37°C, 5% CO_2). The supernatant of cells was either replaced with 50 μg/mL hVLDL in DMEM or fresh DMEM. After 20 h (37°C, 5% CO_2), cells were incubated with iron particles (100 μg Fe/mL) small (S) or large (L) in size with different coatings [citrate, dextran, or carboxymethylated (CM) dextran] in DMEM or fresh DMEM for 1 h (37°C, 5% CO_2). Nuclei were stained with Hoechst 33342 (Sigma #B2261) in DMEM for 10 min (37°C, 5% CO_2). After washing with Annexin binding buffer (10 mM HEPES, 140 mM NaCl, 5 mM $CaCl_2$; pH 7.37), cells were incubated with 2.5 ng/μL Annexin V for 15 min (37°C, 5% CO_2). Cells were imaged using the BD Pathway 855 (BD Biosciences) and analysed with CellProfiler software 4.0.4.[35]

2.18 Statistical analysis

Data are expressed as mean ± SEM. Normal distribution was assessed by Shapiro–Wilkes normality test, followed by Student's *t*-test or ANOVA for normal distributed data or a non-parametric Mann–Whitney *U* test or Kruskal–Wallis to compare two or more groups. Sidak or Dunn's multiple comparison test followed significant changes demonstrated by ANOVA or Kruskal–Wallis, respectively. Results were considered statistically different when $P < 0.05$.

3. Results

3.1 Iron oxide nanoparticles induce macrophage foam cell apoptosis *in vitro*, plaque, liver, and spleen *in vivo*

RAW264.7 foam cells were formed by preloading with 50 μg/mL hVLDL for 20 h. Ninety-minute treatment with the dextran-coated

Downloaded from https://academic.oup.com/cardiovascres/advance-article/doi/10.1093/cvr/cvac032/6553202 by Jacob Heeren user on 09 November 2022

USPIO ferumoxtran (100 μg Fe/mL) increased apoptosis of foam cells compared with normolipidaemic RAW macrophages (*Figure 1A*) in a time- and hVLDL concentration-dependent manner (*Figure 1E*). Specifically, foam cells showed apoptotic morphology (blebbing and shrinkage) and four-fold enhanced TUNEL positivity (*Figure 1A–C*), despite similar iron uptake as normolipidaemic macrophages (*Figure 1D*). Together, these data indicate that ferumoxtran preferentially induced apoptosis in lipid-laden foam cells.

These findings were confirmed *in vivo* in ApoE$^{-/-}$ mice fed a WTD for 9 weeks before receiving a single dose of the SPIO platform ferumoxide (0.3 mg Fe/kg), of ferumoxtran (1 mg Fe/kg), or saline. Even these subclinical doses of ferumoxide or ferumoxtran markedly enhanced TUNEL-positive apoptosis in atherosclerotic plaque compared with saline controls (*Figure 2A–D*). As expected from the short follow-up time, plaque size was not affected 24 h after treatment (*Figure 2E*), also excluding that observed effects were biased by differences in plaque stage.

3.2 Superparamagnetic iron oxide nanoparticles induce apoptosis in murine liver and spleen *in vivo*

Notably, apoptosis was not only limited to atherosclerotic plaques, as macrophage-rich liver and spleen of ApoE$^{-/-}$ mice also showed significant 2.5–4-fold increases in TUNEL-positive cells after only a single dose of ferumoxide or ferumoxtran treatment (*Figure 2F and G*). TUNEL-positive cells in the spleen were exclusively localized in the red pulp area (Supplementary material online, *Figure S2*), which harbours mainly marginal metallophilic macrophages. These data clearly show that ferumoxide and ferumoxtran treatment both enhance apoptosis in atherosclerotic lesions and other macrophage-rich tissue in hyperlipidaemic mice.

3.3 Repeated iron oxide injections show smaller, but less stable plaques

The effect of ferumoxtran on atherosclerotic lesion progression was studied in LDLR$^{-/-}$ mice, fed a WTD for 3 weeks to develop initial lesions and then subjected to weekly ferumoxtran injections (1 mg Fe/kg) for another 5 weeks. Ferumoxtran-treated mice again showed a 5.4-fold increase in TUNEL-positive plaque cells compared with controls (*Figure 2H–J*). Most apoptotic cells were foam cells, and few endothelial and smooth muscle cells, as inferred from cell morphology and location. Repeated ferumoxtran treatment prevented weight gain, but increased serum levels of total, VLDL, and LDL cholesterol (Supplementary material online, *Figure S3*). These findings are in agreement with a study showing that selective depletion of monocytes/macrophages in circulation and peripheral tissue results in increased (V)LDL-derived cholesterol levels with reduced atherogenesis.[36] Indeed, atherosclerotic plaque size was reduced in ferumoxtran-treated mice (*Figure 2K*), despite the moderate serum cholesterol increase. This observation concurs with known effects of enhanced apoptosis on early atherosclerosis.[2] Notwithstanding increased apoptosis, plaque macrophage content was increased in ferumoxtran-treated mice (*Figure 2L*), possibly reflective of the influx of new phagocytes upon apoptotic eat-me signals.

3.4 Antioxidant treatment prevents iron oxide nanoparticle-induced apoptosis *in vitro* and *in vivo*

As iron oxide metabolism has been suggested to lead to oxidative stress,[26,27] we investigated whether this could explain ferumoxtran-induced apoptosis. Twenty-four hours after ferumoxtran injection, serum antioxidant levels were increased as shown by increased uric acid concentration with a consequential increase in TEAC (*Figure 3A and B*), a common response to oxidative stress exposure.[37] Uric acid is an established oxidative stress marker. Although uric acid was previously shown to display moderate antioxidant activity, this seems outweighed by its pro-oxidant and pro-inflammatory effects.[38] In addition, plaque oxidant damage (8OH-dG) showed a trend to increase (data not shown), and quantitative RT–PCR of ferumoxtran-treated and control foam cells revealed a strong up-regulation of oxidative stress-related p22phox (also known as neutrophil cytochrome b light chain), and the pro-apoptotic BCL2 associated X, apoptosis regulator (BAX), and X-linked inhibitor of apoptosis genes (*Figure 3C*). Although nanoparticle-induced ROS have been shown to activate the NLR Family Pyrin Domain (NLRP3) inflammasome,[39] ferumoxtran did neither enhance serum interleukin-1β (IL-1β), nor mRNA expression of IL-1β and NLRP3 in liver and spleens *in vivo* (data not shown).

Importantly, ferumoxtran-augmented apoptosis could be prevented by EUK-8 and its more lipophilic O-methyl derivative EUK-134, both antioxidants with superoxide dismutase, catalase, and oxyradical scavenging properties.[40] Antioxidant treatment resulted in normalization of ferumoxtran-induced apoptosis *in vitro* (*Figure 3D*), as well as in LDLR$^{-/-}$ mice with advanced atherosclerosis (*Figure 3E–J*).

3.5 Superparamagnetic iron oxide nanoparticles are associated with enhanced human plaque apoptosis

As ferumoxtran has been widely used as a contrast agent for MRI detection of inflammatory human atherosclerosis,[4,5] the potential impact of ferumoxtran treatment on the human disease was studied in carotid endarterectomy samples. Samples were collected from symptomatic patients that had received ferumoxtran (2.6 mg Fe/kg IV, $n = 9$) 2–11 days prior to surgery, and from control patients ($n = 9$), matched for sex, age, and plaque phenotype (*Table 1*).[4] All patients were eligible, gave informed consent, and completed all steps of the protocol, and were thus included in the analysis. Notably, the dose used in our mouse model experiments was almost three times lower than that used for the clinical study. Electron microscopy detected ferumoxtran mainly in macrophages and smooth muscle cells (*Figure 4A–C*). The percentage of TUNEL-positive apoptotic cells {*Figure 3D–J*; 3.7 ± 1.4 [95% confidence interval (CI) of mean: 0.5–6.9] vs. 18.2 ± 5.3 (95% CI: 5.9–30.5) for the control and ferumoxtran group, respectively}, as well as the number of apoptotic cells per plaque area [33.4 ± 11.1 (95% CI: 7.9–59.0) vs. 191.2 ± 48.0 (95% CI: 80.5–301.9) for the control and ferumoxtran group, respectively] was increased four-fold in atherosclerotic plaque from ferumoxtran-treated compared with untreated patients. Most apoptotic cells were macrophage foam cells (*Figure 4K and L*). TUNEL-positive cells co-localized with CD68-positive macrophages (*Figure 4E and H*) and activated caspase-3 (*Figure 4F and L*). Thus, the use of ferumoxtran in patients with cardiovascular disease aggravated plaque apoptosis, and possibly subsequent plaque instability.

3.6 New USPIO formulation does not enhance macrophage apoptosis *in vitro* or *in vivo*

The newly developed CM dextran-coated USPIO ferumoxytol has recently been approved by the U.S. Food and Drug Administration to treat anaemia in chronic kidney patients.[41] In light of the initial controversy

Downloaded from https://academic.oup.com/cardiovascres/advance-article/doi/10.1093/cvr/cvac032/6553202 by Jacob Heeren user on 09 November 2022

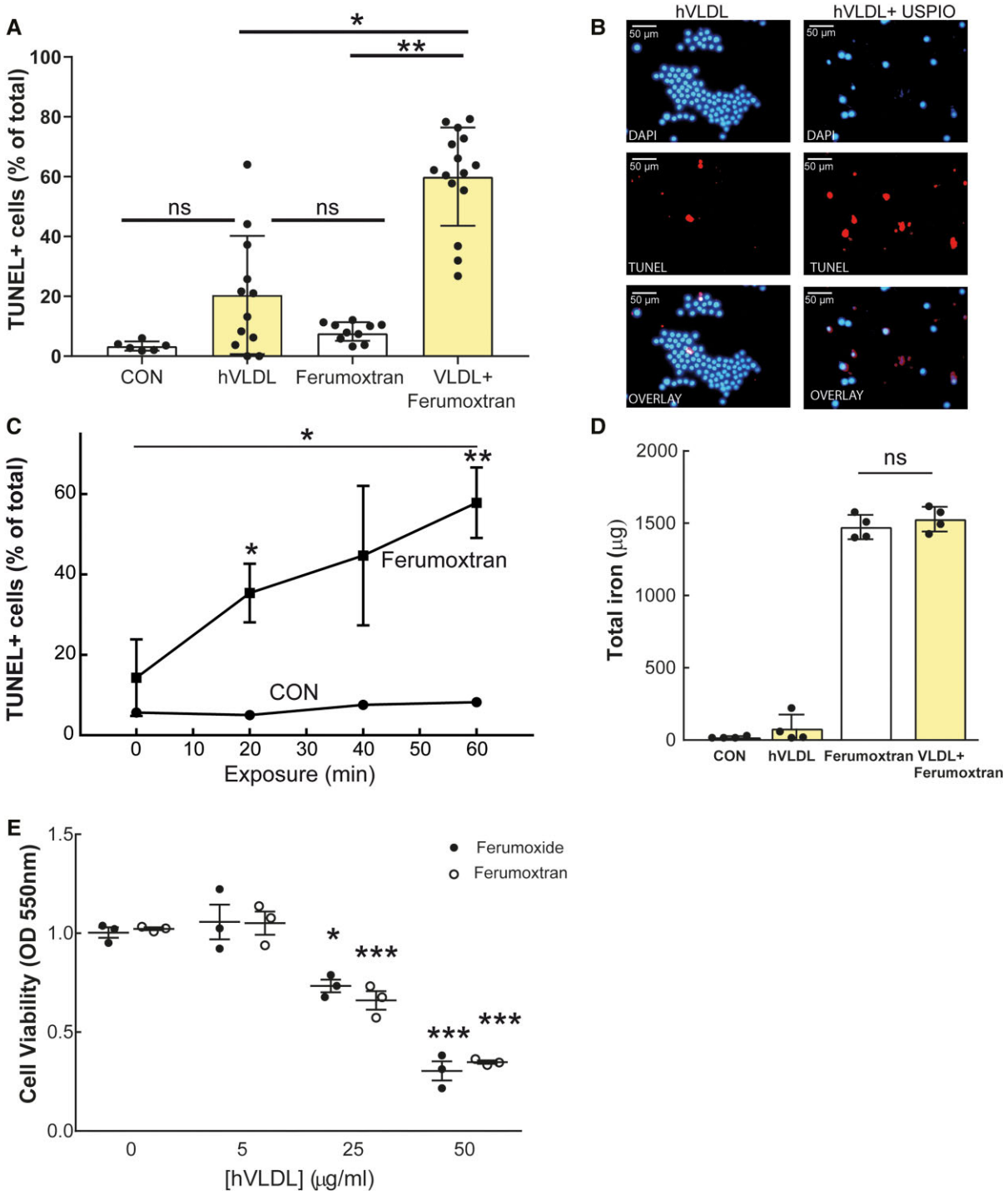

Figure 1 Ferumoxtran exposure increased apoptosis of RAW foam cells compared with normolipidaemic macrophages. (*A*) RAW264.7 cells were transformed into foam cells (20 h incubation with hVLDL 50 µg/mL) and incubated with ferumoxtran (USPIO, 100 µg Fe/mL). (*B*) Fluorescent microscopic pictures of DAPI and TUNEL-stained foam cells incubated with or without ferumoxtran for 1.5 h. (*C*) RAW264.7 control macrophages (circles) and foam cells (squares) were harvested at different time points and cytospins were analysed for TUNEL in three random fields of view (magnification 20×; 412 ± 104 cells/cytospin were analysed). (*D*) The ability of macrophages and foam cells to take up iron-based contrast media was quantitatively analysed using an ICP-AES assay. (*E*) Cell viability after ferumoxide (100 µg Fe/mL, black circles) or ferumoxtran treatment (white circles) of RAW264.7 cells with different lipid loading were determined using a cytotoxic MTT assay. Data are mean ± SEM ($n = 3$), 4–12 technical replicates, and representative of three independent experiments. Statistics: unpaired student's *t*-test, $*P < 0.05$, $**P < 0.01$, and $***P < 0.001$ compared with control conditions. CON, control.

Downloaded from https://academic.oup.com/cardiovascres/advance-article/doi/10.1093/cvr/cvac032/6553202 by Jacob Heeren user on 09 November 2022

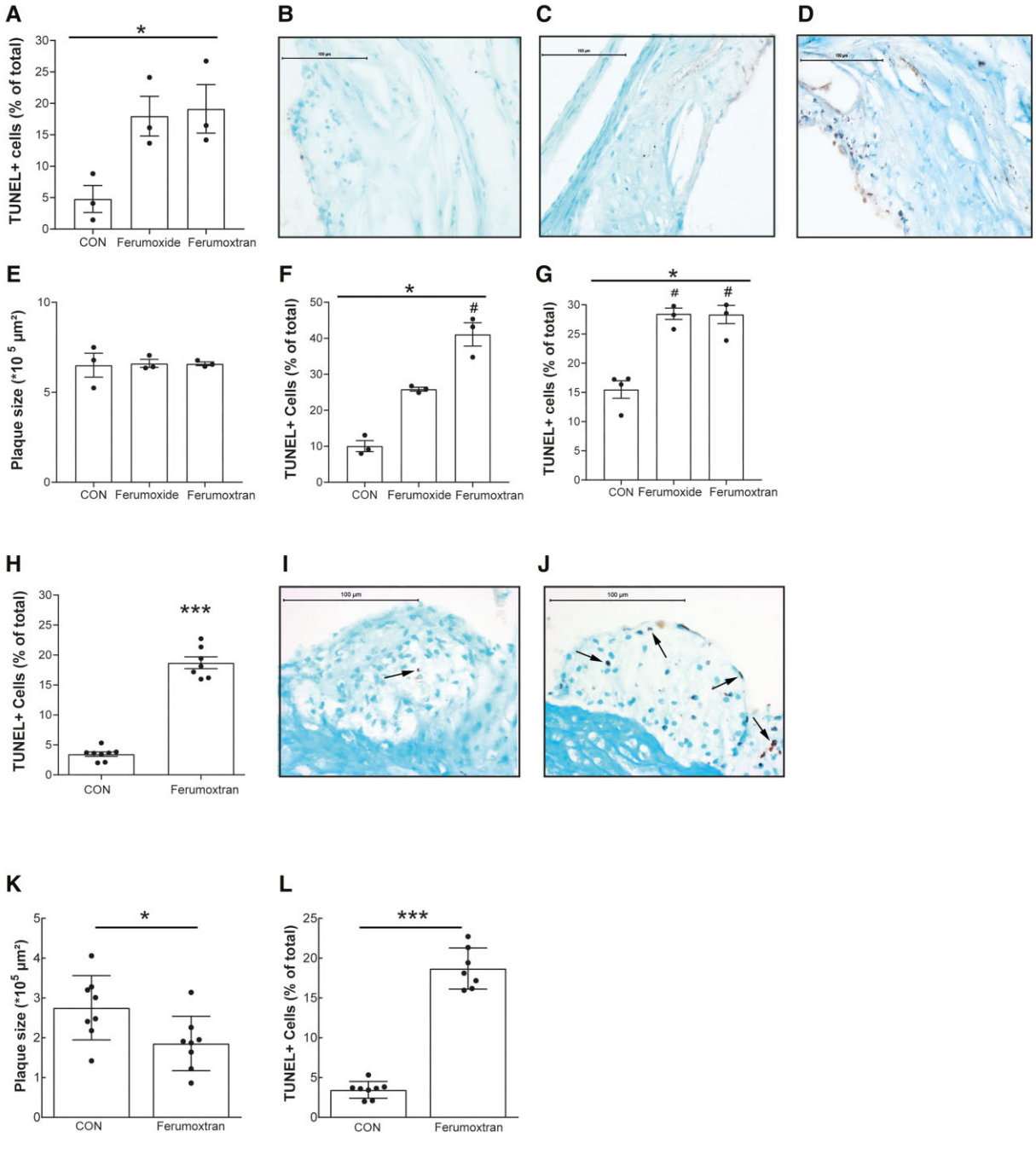

Figure 2 Ferumoxide and ferumoxtran increased apoptosis in atherosclerotic lesions in hyperlipidaemic ApoE$^{-/-}$ and LDLR$^{-/-}$ mice. (*A*) ApoE$^{-/-}$ mice with advanced atherosclerosis were injected once with NaCl 0.9% ($n = 3$), ferumoxide (0.3 mg Fe/kg; $n = 3$), or ferumoxtran (1 mg Fe/kg; $n = 3$). TUNEL-positive cells in the atherosclerotic plaques of the aortic root were quantified and normalized to total cell count. *$P < 0.05$ for Kruskal–Wallis across three groups, no significant changes in Dunn's *post hoc* testing between individual groups. (*B*) Representative image of TUNEL staining of plaques in control, (*C*) ferumoxide, or (*D*) ferumoxtran-treated mice. Scale bar in (*B*) to (*D*) corresponds to 100 µm. (*E*) Plaque area of ApoE$^{-/-}$ was determined by computer-assisted morphometric analysis of Oil red O-stained section. (*F*) The percentage of TUNEL-positive cells was quantified in liver and (*G*) spleen of ApoE$^{-/-}$ mice controls and mice receiving a single ferumoxide or ferumoxtran dose. *$P < 0.05$ for Kruskal–Wallis across three groups, $^{\#}P < 0.05$ in Dunn's *post hoc* testing vs. control. (*H*) LDLR$^{-/-}$ mice with initial plaques were fed a high cholesterol diet and received weekly intravenous injections with NaCl 0.9% (control group, $n = 8$) or ferumoxtran ($n = 8$). The percentage of TUNEL-positive cells was quantified in the atherosclerotic plaques of the aortic root. Unpaired Student's *t*-test, *$P < 0.05$ and ***$P < 0.001$ compared with control conditions. (*I*) Representative image of TUNEL staining of plaques in control and (*J*) ferumoxtran-treated LDLR$^{-/-}$ mice. (*K*) Plaque area (Oil red O) and (*I*) the percentage of macrophages (MoMa-2-positive) cells were quantified in plaques of control LDLR$^{-/-}$ and mice repeatedly treated with ferumoxtran. Statistics: unpaired Student's *t*-test, *$P < 0.05$ and ***$P < 0.001$ compared with control conditions. Data are mean ± SEM. CON, control.

Downloaded from https://academic.oup.com/cardiovascres/advance-article/doi/10.1093/cvr/cvac032/6553202 by Jacob Heeren user on 09 November 2022

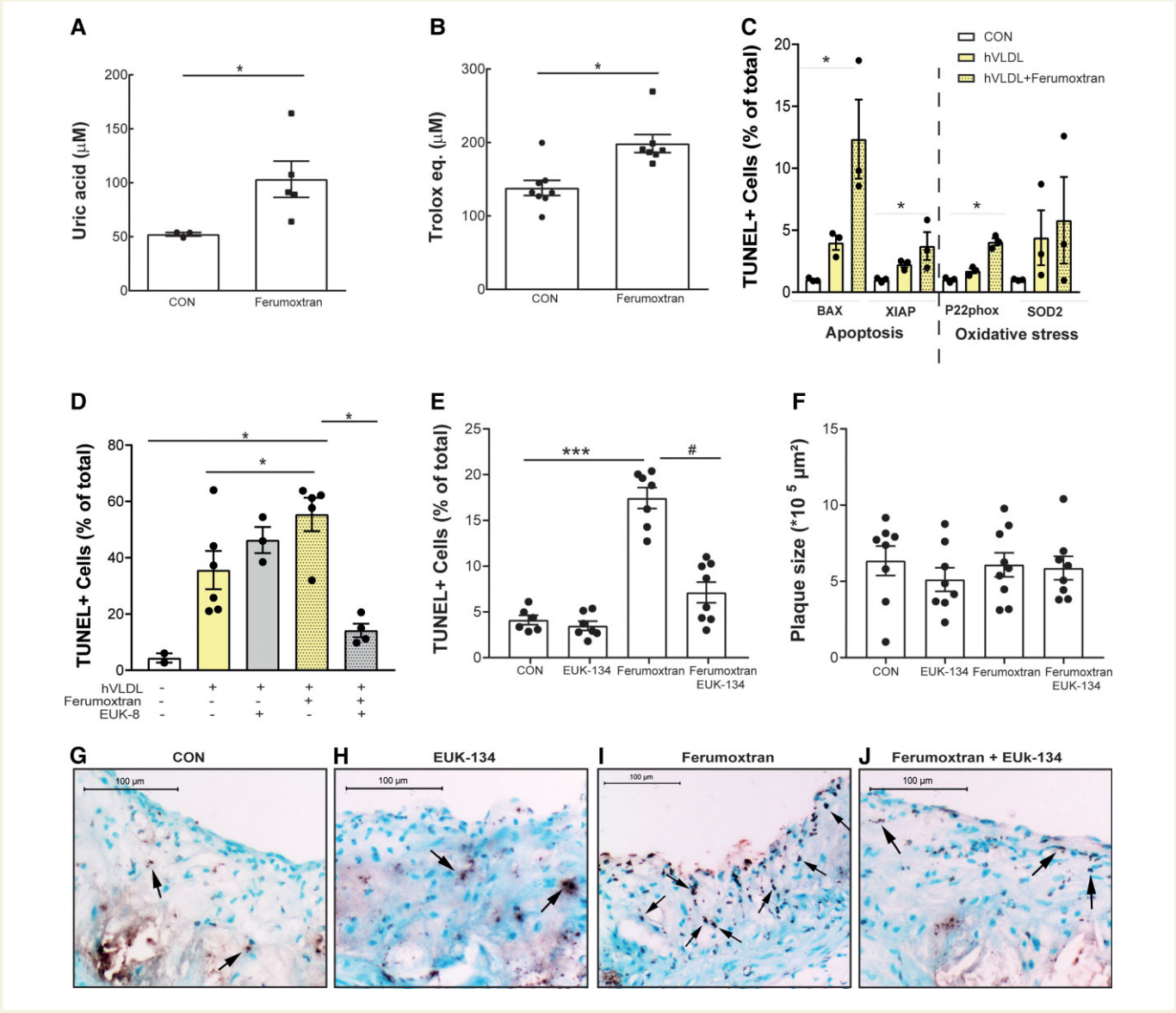

Figure 3 Ferumoxtran triggered ROS-induced apoptosis *in vitro* and *in vivo*. (*A*) Serum uric acid and (*B*) TEAC were increased in serum samples of LDLR$^{-/-}$ mice 24 h after ferumoxtran injection compared with control, a common response to oxidant stress exposure. Statistics: unpaired Student's *t*-test. Data are mean ± SEM. (*C*) Gene expression levels of apoptosis- and oxidative stress-related genes of RAW untreated macrophages (white bars), hVLDL-treated foam cells (yellow bars), and hVLDL-treated foam cells exposed to 100 μg/mL ferumoxtran (yellow dotted bars). (*D*) RAW264.7 cells transformed into foam cells with hVLDL (yellow bars) were incubated with ferumoxtran (dotted filling) to induce apoptosis. Pre-treatment of hVLDL foam cells with antioxidant (grey bars) prior to ferumoxtran reduced apoptosis. Untreated RAW264.7 cells were used as a control (white bars). Cells were harvested, cytospins were made, and apoptotic cells were quantified by TUNEL analysis in four randomly chosen field of views (20× magnification; average 93 ± 27 cells/FOV analysed). Data are mean ± SEM, include 3–6 technical replicates, and are representative of three independent experiments. Statistics: $*P < 0.05$, and $P < 0.001$ vs. control (Kruskal–Wallis; Dunn's multiple comparison). (*E*) LDLR$^{-/-}$ mice on a high cholesterol diet for 6 weeks received a single treatment with either saline ($n = 8$), saline with antioxidant EUK-134 (10 mg/kg, $n = 8$), ferumoxtran alone (1000 μg Fe/kg, $n = 9$), or ferumoxtran with EUK-134 ($n = 9$). The percentage of TUNEL-positive cells was quantified in the atherosclerotic plaques of the aortic root. Statistics: $*P < 0.05$, and $P < 0.001$ vs. control (ANOVA; Sidak's multiple comparison). (*F*) Plaque area (Oil red O) was quantified in plaques of LDLR$^{-/-}$ treated once with saline, EUK-134, ferumoxtran, or ferumoxtran with EUK-134. (*G*) Representative image of TUNEL staining of plaques in saline, (*H*) EUK-134, (*I*) ferumoxtran, or (*J*) ferumoxtran with EUK-134 treated LDLR$^{-/-}$ mice. Data are mean ± SEM. CON, control.

regarding acute side-effects at the time of injection[42] and its use in clinical trials of several cardiovascular diseases,[9,15–19,43] this new generation USPIO was also tested *in vivo* and *in vitro*. In contrast to prior USPIO formulations, ferumoxytol did not enhance apoptosis in plaques or liver of hypercholesterolaemic LDLR$^{-/-}$ mice (*Figure 5A–G*). In line, ferumoxytol did not enhance foam cell apoptosis *in vitro*, despite positive Perl's iron staining (*Figure 5H–J*). This supports a favourable safety profile of ferumoxytol for cardiovascular imaging, in line with recent safety reports,[44] and in contrast to ferumoxtran and ferumoxide, the use of which may have side-effects on atherosclerotic plaque stability.

Downloaded from https://academic.oup.com/cardiovascres/advance-article/doi/10.1093/cvr/cvac032/6553202 by Jacob Heeren user on 09 November 2022

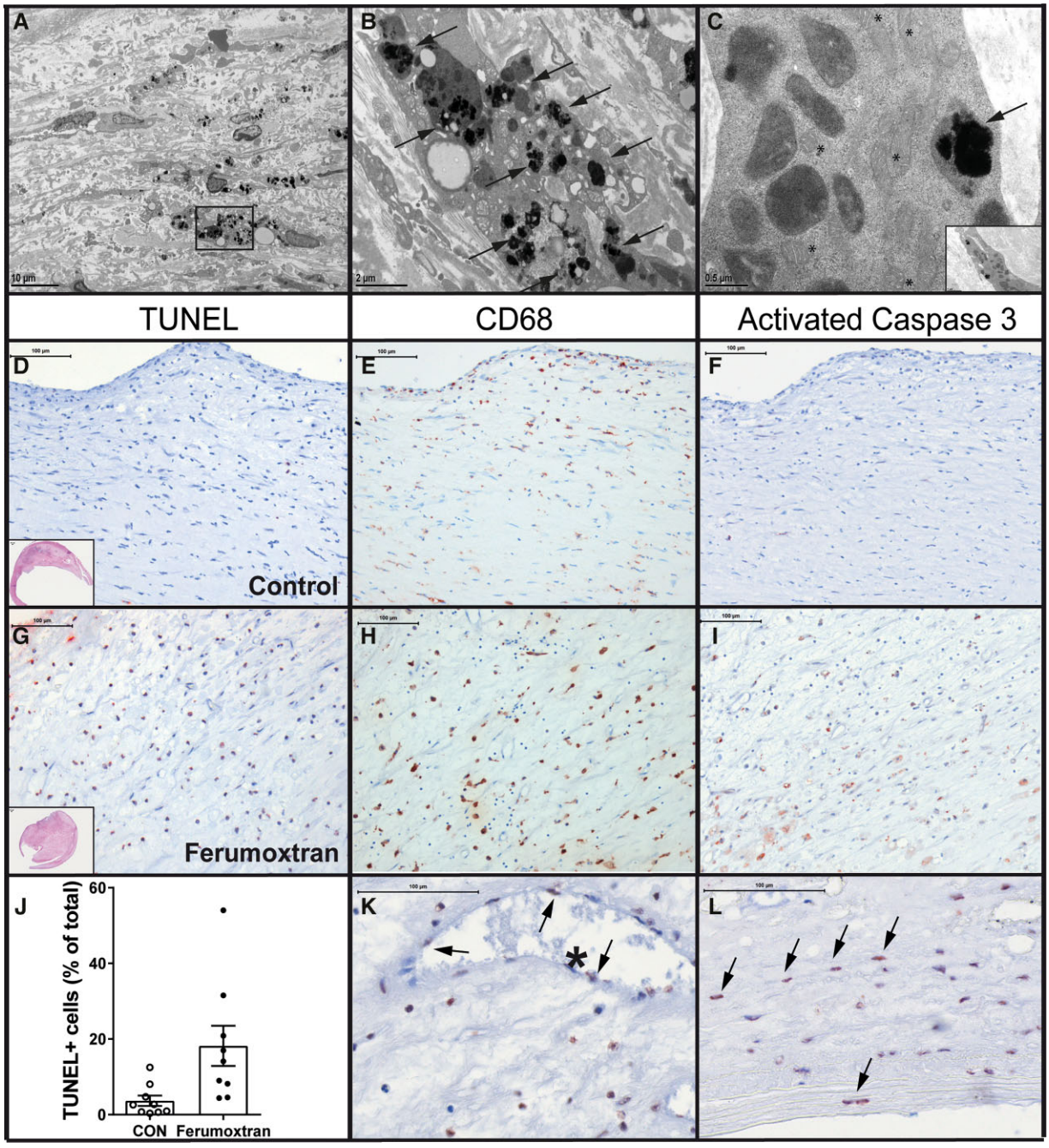

Figure 4 Ferumoxtran increased apoptosis in human carotid atherosclerotic lesions. (*A*) Electron microscopy shows human carotid atherosclerotic plaque with the accumulation of superparamagnetic iron oxide nanoparticles, scale bar corresponds to 10 µm. Boxed region shows particle-laden macrophages, represented in (*B*) high power view of macrophage with intracellular ferumoxtran (arrows). Scale bar corresponds to 2 µm. (*C*) Smooth muscle cell with numerous mitochondria (*) also showing intracellular accumulation of ferumoxtran nanoparticles (arrow). Insert shows the origin of smooth muscle cell. Scale bar corresponds to 0.5 µm. (*D*) Atherosclerotic lesions obtained from symptomatic patients undergoing carotid endarterectomy and receiving no injection ($n = 9$, *D–F*) or a single dose of ferumoxtran (2.7 mg/kg IV, $n = 9$, *G–I*) prior to surgery. Sections were stained with TUNEL (AEC red precipitate, *D*, *G*). Apoptotic TUNEL-positive cells co-localize with macrophages and activated caspase-3 on serial sections stained, respectively, with CD68 (red precipitate; *E*, *H*), (F) activated caspase 3 (red precipitate; *F*, *I*). Scale bars in (*D*)–(*I*) correspond to 100 µm. (*J*) Apoptosis was quantified as TUNEL-positive cells per total cell count. (*K*) Arrows indicate TUNEL-positive nuclei in endothelial cells lining an intraplaque microvessel and (*L*) smooth muscle cells. Scale bars in (*K*) and (*L*) correspond to 100 µm. Data are mean ± SEM. Statistics: $^{**}P = 0.004$ (Mann–Whitney compared with control). CON, control.

Downloaded from https://academic.oup.com/cardiovascres/advance-article/doi/10.1093/cvr/cvac032/6553202 by Jacob Heeren user on 09 November 2022

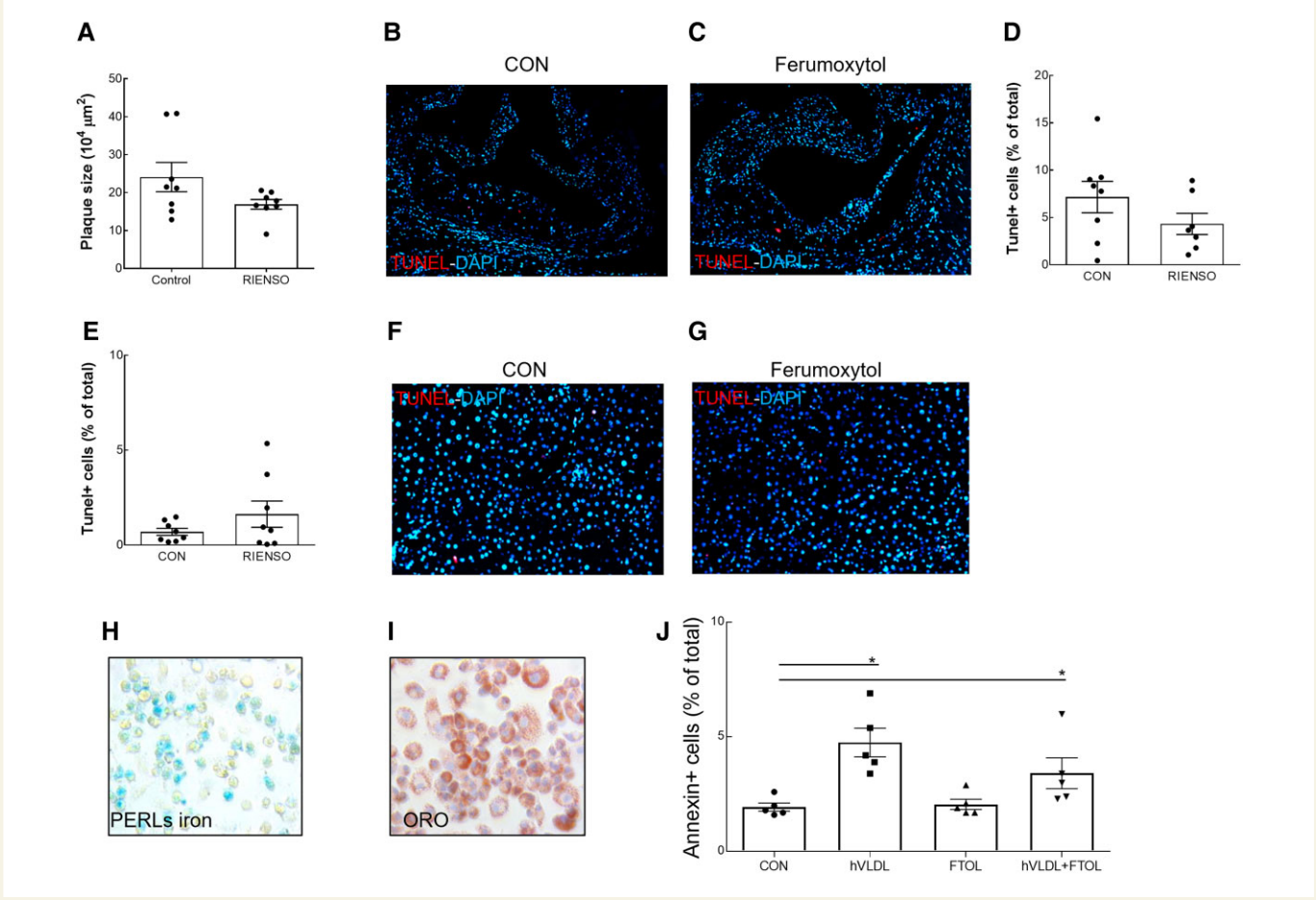

Figure 5 Ferumoxytol did not enhance apoptosis *in vivo* or *in vitro*. (*A*) Plaque area at sacrifice of LDLR$^{-/-}$ mice with early atherosclerosis which were fed a high cholesterol diet for 9 weeks after single weekly IV injections with NaCl 0.9% (control group, $n = 8$) or ferumoxytol ($n = 8$). Representative images of apoptotic cells detected by TUNEL in atherosclerotic plaques of the aortic root of LDLR$^{-/-}$ mice injected with saline (control, *B*) or ferumoxytol (*C*), with corresponding quantification (*D*). Quantification (*E*) and representative images of apoptotic cells detected by TUNEL in liver of LDLR$^{-/-}$ mice injected with saline (control, *F*) or ferumoxytol (*G*). (*H*) Perl's iron staining of RAW cells, incubated with hVLDL and ferumoxytol, detects iron accumulation. (*I*) Oil red O staining of RAW cells, incubated with hVLDL and ferumoxytol, confirmed massive lipid accumulation. (*J*) The percentage of apoptotic, Annexin V-positive cells was quantified by flow cytometry of RAW cells incubated with or without hVLDL, in the absence or presence of ferumoxytol ($n = 5$–8 technical replicates per group). Data are mean ± SEM. *$P < 0.05$, (unpaired Mann–Whitney test or Kruskal–Wallis with Dunn's multiple comparison test, compared with control). CON, control.

3.7 Dextran coating and particle size are not associated with enhanced macrophage apoptosis

Since ferumoxide and ferumoxtran particles are coated with dextran, while ferumoxytol particles are coated with negatively charged CM dextran, the effect of iron particle coating on macrophage apoptosis was investigated. Dextran was avidly taken up by RAW264.7 macrophages (*Figure 6A and B*) but, compared with the untreated control, no significant induction of apoptosis in both foam cells and normolipidaemic macrophages was observed (*Figure 6C and D*). Moreover, no significant difference in apoptosis was observed in both normolipidaemic and hVLDL-laden RAW264.7 cells incubated with iron nanoparticles coated with citrate, dextran, or CM dextran (Supplementary material online, *Figure S4*). Particle size itself also did not appear to be a major determinant of USPIO-induced apoptosis (Supplementary material online, *Figure S4 and Table S2*). Taken together, these findings suggest that neither particle size nor coating accounts for the difference in apoptosis induction found between ferumoxtran and ferumoxytol.

4. Discussion

Collectively, our findings indicate that the administration of previous formulations of superparamagnetic iron oxide nanoparticles enhances apoptosis in murine and human atherosclerosis. Despite the large body of evidence supporting the safety of superparamagnetic iron oxide nanoparticles,[22,23] concern is growing that (U)SPIO uptake may lead to intracellular release of iron ions, generation of oxidative stress, and DNA damage, and that it will promote thrombogenicity in the heart.[26,45,46] Our study shows that ferumoxide and ferumoxtran induce apoptosis and ROS in lipid-laden macrophages and that its effects can be prevented by antioxidant treatment *in vivo* and *in vitro*, pointing to iron oxide-induced oxidative stress as a causative factor for

Downloaded from https://academic.oup.com/cardiovascres/advance-article/doi/10.1093/cvr/cvac032/6553202 by Jacob Heeren user on 09 November 2022

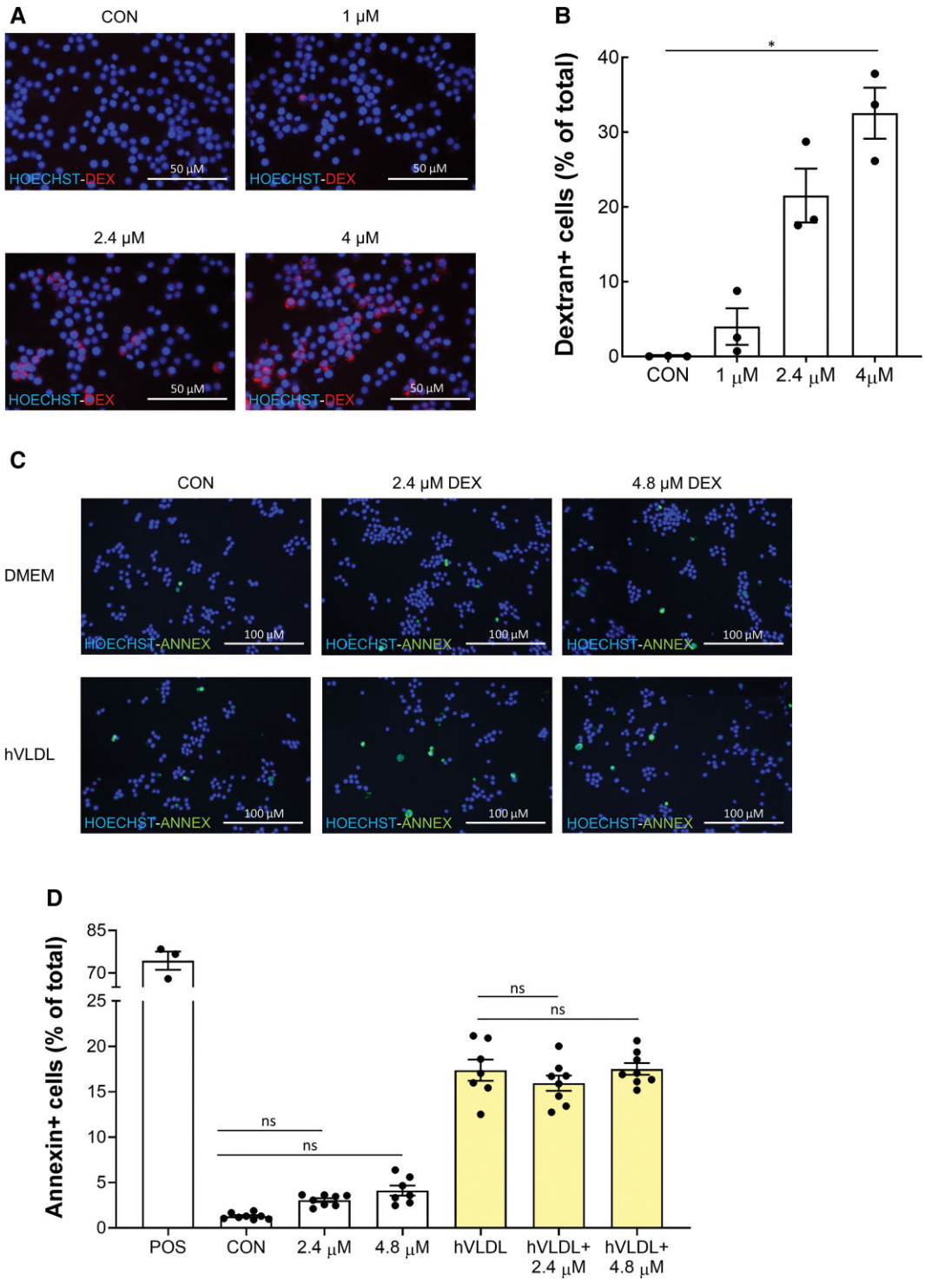

Figure 6 Dextran does not increase apoptosis in RAW foam cells compared with normolipidaemic macrophages. (*A*) Fluorescent microscopic pictures of RAW264.7 incubated with 1, 2.4, or 4 μM TRITC-dextran for 1 h or untreated RAW264.7 (CON) and stained with Hoechst 33342. Per well, nine fluorescent images were taken and merged, corresponding to around 2700 cells imaged per well, with three technical replicates per condition. Scale bars correspond to 50 μm. (*B*) Quantification of (*A*), percentage of cells positive for TRITC-dextran. (*C*) Fluorescent microscopic pictures of RAW264.7 transformed into foam cells with hVLDL (yellow bars) or normolipidaemic cells (white bars) exposed to 2.4 or 4.8 μM dextran or fresh DMEM for 1 h. Untreated cells served as control (CON), RAW264.7 cells treated with 1 μM staurosporine for 20 h served as positive control (POS). Cells were stained with Annexin V and Hoechst 33342. 9 fluorescent images were taken and merged per well, corresponding to around 4400 cells imaged per well, with 3 (POS) or 7–8 technical replicates per condition. Scale bars correspond to 100 μm. (*D*) Quantification of (*C*), percentage of cells positive for Annexin V. Data are presented as mean ± SEM and representative of three independent experiments (*C*, *D*). Statistics: $*P < 0.05$ (Kruskal–Wallis with Dunn's multiple comparison test).

Downloaded from https://academic.oup.com/cardiovascres/advance-article/doi/10.1093/cvr/cvac032/6553202 by Jacob Heeren user on 09 November 2022

Table 2 Nanoparticle characteristics

Feature	Ferumoxide	Ferumoxtran	Ferumoxytol
SPIO/USPIO	SPIO	USPIO	USPIO
Particle size (nm)	120–180	31 ± 5	28 ± 4
Crystal core size (nm)	5	6	6.7
Polydispersity index	n.a.	0.374 ± 0.019	0.252 ± 0.018
Half-life (h)	2–3	30	15
Coating	Dextran	Dextran	Carboxymethyl dextran
Zeta potential ζ (mV)	n.a.	−27 ± 7.1	−43.9 ± 8.4
Macrophage uptake (pg Fe/cell)[a]	5.0–7.0	0.5–1.8	1.0–1.5
Mechanism uptake	SRA1	SRA1	SRA1
Clinical dose mg/kg	0.6	4	2.7

Integrated data from Refs.[61–64] and own measurements. SRA1, scavenger-receptor A mediated; n.a., information not available.
[a]THP-1 with 200 μg Fe/mL for 24 h.

USPIO-induced apoptosis. In support of this finding, bare USPIO was seen to induce endothelial cell apoptosis *in vitro*, which was also mediated by USPIO-related ROS, and reversed by antioxidant treatment.[47,48] In fact, we observed occasional endothelial apoptosis in atherosclerotic plaque after treatment with dextran-coated ferumoxide (SPIO), and to a lesser extent ferumoxtran (USPIO). The apparent preference for foam cell apoptosis may be explained by the increased susceptibility to apoptosis of lipid-laden foam cells subjected to a second stressor.[24]

Moreover, repeated ferumoxtran treatment of mice with early atherosclerosis not only led to enhanced plaque apoptosis but also increased plaque macrophage accumulation. Interestingly, this did not translate in progressive plaque growth. Although the jury is still out on this notion, increased macrophage apoptosis has indeed been suggested to impede plaque progression in early-stage atherosclerosis as phagocytic clearance of apoptotic cells is fully operative at this stage.[36,49,50] In contrast, in advanced plaques with compromised efferocytosis,[51] accumulating apoptotic cell debris and secondary necrosis will directly promote plaque progression by the expansion of the necrotic core and inflammation.[2,52] As ferumoxtran exacerbated plaque apoptosis in mice and patients with advanced atherosclerosis, this raises concerns regarding potentially deleterious effects on plaque progression and destabilization. This is especially true considering the prolonged residence time of USPIO platforms in tissue. In fact, in porcine heart, USPIO persisted for several months after intracardiac injection of USPIO-labelled stem cells.[53] However, our CVD cohort, with its limited group size, is not fit to draw any conclusions on USPIO treatment-associated clinical adverse events.

Considering the widespread cardiovascular and non-cardiovascular clinical use of USPIO, our findings may have a broader impact. USPIO-based imaging has been used for the diagnosis of tumour metastases, autoimmune diseases, rheumatoid arthritis, for targeted stem cell transfer to the infarcted heart, and for treatment of anaemia in patients with chronic kidney disease.[23,53–55] Although ferumoxtran has been discontinued in 2010,[53–56] several trials have been started to test the potential of similar USPIO platforms for the diagnosis of prostate cancer,[53–57,53–58] head and neck squamous cell carcinoma,[53–59] and aortic dissection.[60] Most applications involve elderly patient populations, expected to suffer from moderate to advanced atherosclerosis. Nevertheless, ferumoxytol, a new generation USPIO equipped with a CM dextran coating, appears to display a safer profile for cardiovascular disease. Biodistribution, macrophage uptake route and speed, and intracellular release of USPIO entrapped iron are dependent on particle and iron core size and composition, coating chemistry, and charge and will define the particle's pro-oxidant and pro-apoptotic activity. Dextran-coated SPIOs ferumoxide and ferumoxtran, while differently sized, both acted pro-apoptotic, suggesting that coating (chemistry) may be critical (*Table 2*).[61–63] However, it has previously been shown that blocking CD206 or CD11b does not reduce SPIO uptake by macrophages, indicating that interaction of the dextran coating with carbohydrate receptors does not notably contribute to SPIO uptake.[65] Our data show that dextran polymers of similar size and molecular concentration as the derived SPIO were completely inert, suggesting that particle charge or subtle factors in the SPIO production process may be critical. Net macrophage uptake (and thus gross iron oxide availability) of ferumoxide was highest, followed by ferumoxytol and ferumoxtran,[61,66] which underpins that particle intrinsic factors are decisive. Ferumoxytol uptake, while higher than that of ferumoxtran, did not enhance apoptosis. As ferumoxytol and ferumoxtran differ in coating chemistry and charge (negatively charged CM dextran vs. non-ionic dextran[63]), but not in particle size and core composition, this suggests that the former factors are indeed instrumental in its toxicity. The lack of toxicity of citrate- vs. dextran- vs. CM dextran-coated USPIO particles[34] of similar size, suggest however that the driving determinant may be even more subtle, and relate to differences in coating density or heterogeneity. Nevertheless, our study may reassure recent investigators and their patients on safe use of ferumoxytol.[9,16,17,23,43,44,66]

In conclusion, iron-based contrast agents, such as ferumoxide and ferumoxtran increase apoptosis in human and murine atherosclerotic plaque, an effect that can be prevented by antioxidants. Their administration to patients with advanced lesions may result in plaque destabilization. Although ferumoxytol appears to have a safe cardiovascular profile, our findings indicate that caution should be exercised when applying other iron-based contrast agents in patients with clinical atherosclerosis or other inflammatory disorders that involve lipid-laden macrophages.

Supplementary material

Supplementary material is available at *Cardiovascular Research* online.

Author contributions

F.M.E.S., T.J.C.v.B., and E.A.L.B. were responsible for conception and design. All authors were involved in analysis and interpretation of data. F.M.E.S., A.V.R., I.B., T.J.C.v.B., B.H., J.C.S., and E.A.L.B. drafted the manuscript, or revised it critically for important intellectual content. All authors gave final approval of the submitted manuscript and agree to be accountable for all aspects of the work in ensuring that questions related to the accuracy or integrity of any part of the work are appropriately investigated and resolved.

Conflicts of interest: The principal investigator (E.A.L.B.) has received financial support for this work from Guerbet. This manuscript was handled by Consulting Editor Alain Tedgui.

Downloaded from https://academic.oup.com/cardiovascres/advance-article/doi/10.1093/cvr/cvac032/6553202 by Jacob Heeren user on 09 November 2022

Funding

This work was supported by the Dutch Heart Foundation (established investigator Hartstichting 2003T201 to E.A.L.B., senior postdoc 2016T060 to J.C.S.); Guerbet; two VENI fellowships (916.86.04 to I.B., 016.116.017 to J.C.S.); a VIDI fellowship of the Netherlands Organization of Scientific Research (0.16.186.364 to J.C.S.); an European Research Council consolidator grant (864121 to T.L.); the German Research Foundation (GRK/RTG2375: 331065168 to T.L.); and the Fondation Leducq transatlantic network of excellence 'Modulating autophagy to treat CVD' (15CVD04 to J.C.S).

Data availability

The data underlying this article are available in the article and in its online supplementary material.

References

1. Fayad ZA, Fuster V, Fallon JT, Jayasundera T, Worthley SG, Helft G, Aguinaldo JG, Badimon JJ, Sharma SK. Noninvasive in vivo human coronary artery lumen and wall imaging using black-blood magnetic resonance imaging. *Circulation* 2000;**102**:506–510.
2. Moore KJ, Tabas I. Macrophages in the pathogenesis of atherosclerosis. *Cell* 2011;**145**:341–355.
3. Virmani R, Kolodgie FD, Burke AP, Finn AV, Gold HK, Tulenko TN, Wrenn SP, Narula J. Atherosclerotic plaque progression and vulnerability to rupture angiogenesis as a source of intraplaque hemorrhage. *Arterioscler Thromb Vasc Biol* 2005;**25**:2054–2061.
4. Kooi ME, Cappendijk VC, Cleutjens KB, Kessels AGH, Kitslaar PJEHM, Borgers M, Frederik PM, Daemen MJAP, van Engelshoven JMA. Accumulation of ultrasmall superparamagnetic particles of iron oxide in human atherosclerotic plaques can be detected by in vivo magnetic resonance imaging. *Circulation* 2003;**107**:2453–2458.
5. Trivedi RA, U-King-Im J-M, Graves MJ, Cross JJ, Horsley J, Goddard MJ, Skepper JN, Quartey G, Warburton E, Joubert I, Wang L, Kirkpatrick PJ, Brown J, Gillard JH. In vivo detection of macrophages in human carotid atheroma: temporal dependence of ultrasmall superparamagnetic particles of iron oxide-enhanced MRI. *Stroke* 2004;**35**:1631–1635.
6. Ruehm SG, Corot C, Vogt P, Kolb S, Debatin JF. Magnetic resonance imaging of atherosclerotic plaque with ultrasmall superparamagnetic particles of iron oxide in hyperlipidemic rabbits. *Circulation* 2001;**103**:415–422.
7. Briley-Saebo KC, Mani V, Hyafil F, Cornily JC, Fayad ZA. Fractionated Feridex and positive contrast: in vivo MR imaging of atherosclerosis. *Magn Reson Med* 2008;**59**:721–730.
8. Zheng KH, Schoormans J, Stiekema LCA, Calcagno C, Cicha I, Alexiou C, Strijkers GJ, Nederveen AJ, Stroes ESG, Coolen BF. Plaque permeability assessed with DCE-MRI associates with USPIO uptake in patients with peripheral artery disease. *JACC Cardiovasc Imaging* 2019;**12**:2081–2083.
9. Smits LP, Tiessens F, Zheng KH, Stroes ES, Nederveen AJ, Coolen BF. Evaluation of ultrasmall superparamagnetic iron-oxide (USPIO) enhanced MRI with ferumoxytol to quantify arterial wall inflammation. *Atherosclerosis* 2017;**263**:211–218.
10. Dadfar SM, Roemhild K, Drude NI, von Stillfried S, Knüchel R, Kiessling F, Lammers T. Iron oxide nanoparticles: diagnostic, therapeutic and theranostic applications. *Adv Drug Deliv Rev* 2019;**138**:302–325.
11. Hanini A, Schmitt A, Kacem K, Chau F, Ammar S, Gavard J. Evaluation of iron oxide nanoparticle biocompatibility. *Int J Nanomed* 2011;**6**:787–794.
12. von zur Muhlen C, von Elverfeldt D, Bassler N, Neudorfer I, Steitz B, Petri-Fink A, Hofmann H, Bode C, Peter K. Superparamagnetic iron oxide binding and uptake as imaged by magnetic resonance is mediated by the integrin receptor Mac-1 (CD11b/CD18): implications on imaging of atherosclerotic plaques. *Atherosclerosis* 2007;**193**:102–111.
13. Olzinski AR, Turner GH, Bernard RE, Karr H, Cornejo CA, Aravindhan K, Hoang B, Ringenberg MA, Qin P, Goodman KB, Willette RN, Macphee CH, Jucker BM, Sehon CA, Gough PJ. Pharmacological inhibition of C–C chemokine receptor 2 decreases macrophage infiltration in the aortic root of the human C–C chemokine receptor 2/apolipoprotein E−/− mouse: magnetic resonance imaging assessment. *Arterioscler Thromb Vasc Biol* 2010;**30**:253–259.
14. Rogers WJ, Basu P. Factors regulating macrophage endocytosis of nanoparticles: implications for targeted magnetic resonance plaque imaging. *Atherosclerosis* 2005;**178**:67–73.
15. Richards JM, Semple SI, MacGillivray TJ, Gray C, Langrish JP, Williams M, Dweck M, Wallace W, McKillop G, Chalmers RT, Garden OJ, Newby DE. Abdominal aortic aneurysm growth predicted by uptake of ultrasmall superparamagnetic particles of iron oxide: a pilot study. *Circ Cardiovasc Imaging* 2011;**4**:274–281.
16. Stirrat CG, Alam SR, MacGillivray TJ, Gray CD, Dweck MR, Dibb K, Spath N, Payne JR, Prasad SK, Gardner RS, Mirsadraee S, Henriksen PA, Semple SI, Newby DE. Ferumoxytol-enhanced magnetic resonance imaging in acute myocarditis. *Heart* 2018;**104**:300–305.
17. Stirrat CG, Alam SR, MacGillivray TJ, Gray CD, Dweck MR, Raftis J, Jenkins WS, Wallace WA, Pessotto R, Lim KH, Mirsadraee S, Henriksen PA, Semple SI, Newby DE. Ferumoxytol-enhanced magnetic resonance imaging assessing inflammation after myocardial infarction. *Heart* 2017;**103**:1528–1535.
18. MA3RS Study Investigators. Aortic wall inflammation predicts abdominal aortic aneurysm expansion, rupture, and need for surgical repair. *Circulation* 2017;**136**:787–797.
19. Lagan J, Naish JH, Simpson K, Zi M, Cartwright EJ, Foden P, Morris J, Clark D, Birchall L, Caldwell J, Trafford A, Fortune C, Cullen M, Chaudhuri N, Fildes J, Sarma J, Schelbert EB, Schmitt M, Piper Hanley K, Miller CA. Substrate for the myocardial inflammation-heart failure hypothesis identified using novel USPIO methodology. *JACC Cardiovasc Imaging* 2020;**14**:365–376.
20. Trivedi RA, U-King-Im J-M, Graves MJ, Cross JJ, Horsley J, Goddard MJ, Skepper JN, Quartey G, Warburton E, Joubert I, Wang L, Kirkpatrick PJ, Brown J, Gillard JH. In vivo detection of macrophages in human carotid atheroma. *Stroke* 2004; **35**:1631–1635.
21. Müller K, Skepper JN, Posfai M, Trivedi R, Howarth S, Corot C, Lancelot E, Thompson PW, Brown AP, Gillard JH. Effect of ultrasmall superparamagnetic iron oxide nanoparticles (Ferumoxtran-10) on human monocyte-macrophages in vitro. *Biomaterials* 2007;**28**:1629–1642.
22. Bourrinet P, Bengele HH, Bonnemain B, Dencausse A, Idee JM, Jacobs PM, Lewis JM. Preclinical safety and pharmacokinetic profile of Ferumoxtran-10, an ultrasmall superparamagnetic iron oxide magnetic resonance contrast agent. *Invest Radiol* 2006;**41**:313–324.
23. Macdougall IC, Strauss WE, McLaughlin J, Li Z, Dellanna F, Hertel J. A randomized comparison of ferumoxytol and iron sucrose for treating iron deficiency anemia in patients with CKD. *Clin J Am Soc Nephrol* 2014;**9**:705–712.
24. Devries-Seimon T, Li Y, Yao PM, Stone E, Wang Y, Davis RJ, Flavell R, Tabas I. Cholesterol-induced macrophage apoptosis requires ER stress pathways and engagement of the type A scavenger receptor. *J Cell Biol* 2005;**171**:61–73.
25. Hung YC, Hong MY, Huang GS. Cholesterol loading augments oxidative stress in macrophages. *FEBS Lett* 2006;**580**:849–861.
26. Briley-Saebo K, Bjørnerud A, Grant D, Ahlstrom H, Berg T, Kindberg GM. Hepatic cellular distribution and degradation of iron oxide nanoparticles following single intravenous injection in rats: implications for magnetic resonance imaging. *Cell Tissue Res* 2004;**316**:315–323.
27. Fayad ZA, Razzouk L, Briley-Saebo KC, Mani V. Iron oxide magnetic resonance imaging for atherosclerosis therapeutic evaluation: still "rusty?". *J Am Coll Cardiol* 2009;**53**:2051–2052.
28. Guildford AL, Poletti T, Osbourne LH, Di Cerbo A, Gatti AM, Santin M. Nanoparticles of a different source induce different patterns of activation in key biochemical and cellular components of the host response. *J R Soc Interface* 2009;**6**:1213–1221.
29. Redgrave TG, Roberts DCK, West CE. Separation of plasma lipoproteins by density-gradient ultracentrifugation. *Anal Biochem* 1975;**65**:42–49.
30. Virmani R, Kolodgie FD, Burke AP, Farb A, Schwartz SM. Lessons from sudden coronary death: a comprehensive morphological classification scheme for atherosclerotic lesions. *Arterioscler Thromb Vasc Biol* 2000;**20**:1262–1275.
31. Fischer MAJG, Gransier TJM, Beckers LMG, Bekers O, Bast A, Haenen GRMM. Determination of the antioxidant capacity in blood. *Clin Chem Lab Med* 2005;**43**:735–740.
32. Chomczynski P, Sacchi N. Single-step method of RNA isolation by acid guanidinium thiocyanate–phenol–chloroform extraction. *Anal Biochem* 1987;**162**:156–159.
33. Lamprecht MR, Sabatini DM, Carpenter AE. CellProfiler: free, versatile software for automated biological image analysis. *Biotechniques* 2007;**42**:71–75.
34. Dadfar SM, Camozzi D, Darguzyte M, Roemhild K, Varvarà P, Metselaar J, Banala S, Straub M, Güvener N, Engelmann U, Slabu I, Buhl M, van Leusen J, Kögerler P, Hermanns-Sachweh B, Schulz V, Kiessling F, Lammers T. Size-isolation of superparamagnetic iron oxide nanoparticles improves MRI, MPI and hyperthermia performance. *J Nanobiotechnol* 2020;**18**:22.
35. Lamprecht MR, Sabatini DM, Carpenter AE. CellProfiler: free, versatile software for automated biological image analysis. *Biotechniques* 2007;**42**:71–75.
36. Stoneman V, Braganza D, Figg N, Mercer J, Lang R, Goddard M, Bennett M. Monocyte/macrophage suppression in CD11b diphtheria toxin receptor transgenic mice differentially affects atherogenesis and established plaques. *Circ Res* 2007;**100**:884–893.
37. Ames BN, Cathcart R, Schwiers E, Hochstein P. Uric acid provides an antioxidant defense in humans against oxidant- and radical-caused aging and cancer: a hypothesis. *Proc Natl Acad Sci USA* 1981;**78**:6858–6862.
38. Esen AM, Akcakoyun M, Esen O, Acar G, Emiroglu Y, Pala S, Kargin R, Karapinar H, Ozcan O, Barutcu I. Uric acid as a marker of oxidative stress in dilatation of the ascending aorta. *Am J Hypertens* 2011;**24**:149–154.
39. Zhou R, Yazdi AS, Menu P, Tschopp J. A role for mitochondria in NLRP3 inflammasome activation. *Nature* 2011;**469**:221–225.
40. Rong Y, Doctrow SR, Tocco G, Baudry M. EUK-134, a synthetic superoxide dismutase and catalase mimetic, prevents oxidative stress and attenuates kainate-induced neuropathology. *Proc Natl Acad Sci USA* 1999;**96**:9897–9902.
41. Lu M, Cohen MH, Rieves D, Pazdur R. FDA report: ferumoxytol for intravenous iron therapy in adult patients with chronic kidney disease. *Am J Hematol* 2010;**85**:315–319.
42. FDA. *FDA Drug Safety Communication: FDA strengthens warnings and changes prescribing instructions to decrease the risk of serious allergic reactions with anemia drug Feraheme (Ferumoxytol)*. 2016.
43. Usman A, Patterson AJ, Yuan J, Cluroe A, Patterson I, Graves MJ, Gillard JH, Sadat U. Ferumoxytol-enhanced three-dimensional magnetic resonance imaging of carotid atheroma—a feasibility and temporal dependence study. *Sci Rep* 2020;**10**:1808.

Downloaded from https://academic.oup.com/cardiovascres/advance-article/doi/10.1093/cvr/cvac032/6553202 by Jacob Heeren user on 09 November 2022

44. Wetmore JB, Weinhandl ED, Zhou J, Gilbertson DT. Relative incidence of acute adverse events with ferumoxytol compared to other intravenous iron compounds: a matched cohort study. *PLoS One* 2017;**12**:e0171098.
45. Shen Y, Huang Z, Liu X, Qian J, Xu J, Yang X, Sun A, Ge J. Iron-induced myocardial injury: an alarming side effect of superparamagnetic iron oxide nanoparticles. *J Cell Mol Med* 2015;**19**:2032–2035.
46. Nemmar A, Beegam S, Yuvaraju P, Yasin J, Tariq S, Attoub S, Ali BH. Ultrasmall superparamagnetic iron oxide nanoparticles acutely promote thrombosis and cardiac oxidative stress and DNA damage in mice. *Part Fibre Toxicol* 2016;**13**:22.
47. Buyukhatipoglu K, Clyne AM. Superparamagnetic iron oxide nanoparticles change endothelial cell morphology and mechanics via reactive oxygen species formation. *J Biomed Mater Res A* 2011;**96**:186–195.
48. Zhu MT, Wang B, Wang Y, Yuan L, Wang HJ, Wang M, Ouyang H, Chai ZF, Feng WY, Zhao YL. Endothelial dysfunction and inflammation induced by iron oxide nanoparticle exposure: risk factors for early atherosclerosis. *Toxicol Lett* 2011;**203**:162–171.
49. Babaev VR, Chew JD, Ding L, Davis S, Breyer MD, Breyer RM, Oates JA, Fazio S, Linton MF. Macrophage EP4 deficiency increases apoptosis and suppresses early atherosclerosis. *Cell Metab* 2008;**8**:492–501.
50. Boesten LSM, Zadelaar ASM, van Nieuwkoop A, Hu L, Teunisse AFAS, Jochemsen AG, Evers B, van de Water B, Gijbels MJJ, van Vlijmen BJM, Havekes LM, de Winther MPJ. Macrophage p53 controls macrophage death in atherosclerotic lesions of Apolipoprotein E deficient mice. *Atherosclerosis* 2009;**207**:399–404.
51. Schrijvers DM, De Meyer GRY, Kockx MM, Herman AG, Martinet W. Phagocytosis of apoptotic cells by macrophages is impaired in atherosclerosis. *Arterioscler Thromb Vasc Biol* 2005;**25**:1256–1261.
52. Thorp E, Li G, Seimon TA, Kuriakose G, Ron D, Tabas I. Reduced apoptosis and plaque necrosis in advanced atherosclerotic lesions of Apoe−/− and Ldlr−/− mice lacking CHOP. *Cell Metab* 2009;**9**:474–481.
53. Kawamura M, Miyagawa S, Fukushima S, Saito A, Miki K, Ito E, Sougawa N, Kawamura T, Daimon T, Shimizu T, Okano T, Toda K, Sawa Y. Enhanced survival of transplanted human induced pluripotent stem cell-derived cardiomyocytes by the combination of cell sheets with the pedicled omental flap technique in a porcine heart. *Circulation* 2013;**128**(Suppl 1):S87–S94.
54. Harisinghani MG, Barentsz J, Hahn PF, Deserno WM, Tabatabaei S, van de Kaa CH, de la Rosette J, Weissleder R. Noninvasive detection of clinically occult lymph-node metastases in prostate cancer. *N Engl J Med* 2003;**348**:2491–2499.
55. Beckmann N, Falk R, Zurbrügg S, Dawson J, Engelhardt P. Macrophage infiltration into the rat knee detected by MRI in a model of antigen-induced arthritis. *Magn Reson Med* 2003;**49**:1047–1055.
56. Bietenbeck M, Florian A, Sechtem U, Yilmaz A. The diagnostic value of iron oxide nanoparticles for imaging of myocardial inflammation—quo vadis? *J Cardiovasc Magn Reson* 2015;**17**:54.
57. NIH. Ferumoxtran-10-enhanced MRI in prostate cancer patients. https://ClinicalTrials.gov/show/NCT04261777.
58. NIH. Radio guided lymph node dissection in oligometastatic prostate cancer patients. https://ClinicalTrials.gov/show/NCT04300673.
59. NIH. Validation of USPIO-enhanced MRI for detection of lymph node metastases in head and neck carcinoma. https://ClinicalTrials.gov/show/NCT03817307.
60. NIH. Magnetic resonance imaging (MRI) for aortic dissection to visualize inflammation. https://ClinicalTrials.gov/show/NCT03948555.
61. Modo MMJJ, Bulte JWM. *Molecular and cellular MR imaging*. Boca Raton: CRC Press, 2007.
62. Alam SR, Stirrat C, Richards J, Mirsadraee S, Semple SI, Tse G, Henriksen P, Newby DE. Vascular and plaque imaging with ultrasmall superparamagnetic particles of iron oxide. *J Cardiovasc Magn Reson* 2015;**17**:83.
63. Wang G, Serkova NJ, Groman EV, Scheinman RI, Simberg D. Feraheme (ferumoxytol) is recognized by proinflammatory and anti-inflammatory macrophages via scavenger receptor type AI/II. *Mol Pharm* 2019;**16**:4274–4281.
64. Said B, McCart JA, Libutti SK, Choyke PL. Ferumoxide-enhanced MRI in patients with colorectal cancer and rising CEA: surgical correlation in early recurrence. *Magn Reson Imaging* 2000;**18**:305–309.
65. Chao Y, Karmali PP, Simberg D. Role of carbohydrate receptors in the macrophage uptake of dextran-coated iron oxide nanoparticles. *Adv Exp Med Biol* 2012;**733**:115–123.
66. Yancy AD, Olzinski AR, Hu TC-C, Lenhard SC, Aravindhan K, Gruver SM, Jacobs PM, Willette RN, Jucker BM. Differential uptake of Ferumoxtran-10 and Ferumoxytol, ultrasmall superparamagnetic iron oxide contrast agents in rabbit: critical determinants of atherosclerotic plaque labeling. *J Magn Reson Imaging* 2005;**21**:432–442.

Downloaded from https://academic.oup.com/cardiovascres/advance-article/doi/10.1093/cvr/cvac032/6553202 by Jacob Heeren user on 09 November 2022